Table 1 Nodal cilia features in different vertebrate classes

	Onset of Lrdr mRNA expression	*Appearance of nodal cilia*	*Earliest conserved asymmetric gene expression*
Mouse	Gastrula, 7.5 d.p.f.	Gastrula, 7.5 d.p.f.	*Nodal*, 8.25 d.p.f., 3–5 somites
Chick	Gastrula, HH4 –	Gastrula, HH4 –	*Nodal*, HH7*, 0–2 somites
Xenopus	Stage-11 gastrula	Stage-14 neurula	*Xnr-1* (*Nodal*), stage-17 neurula
Zebrafish	80% epiboly gastrula	Four somites	*Cyclops* (*Nodal*), 20 somites

*Asymmetric gene expression of *Sonic hedgehog* at the node occurs at HH5 (gastrulation) before *Nodal* expression, but seems to be unique to the chick embryo. d.p.f., days post-fertilization.

localization of *Lrdr* expression and formation of nodal cilia. The earliest known asymmetric expression patterns that are common to all vertebrates likewise exhibit considerable variability in their time of onset among different vertebrate classes[1,2]. In all instances, however, these conserved asymmetries are preceded by the onset of *Lrdr* expression and by the appearance of nodal cilia (Table 1), indicating that nodal cilia may be responsible for initiating L–R asymmetric gene expression and for establishing the final body plan in all vertebrates.

Jeffrey J. Essner*, Kyle J. Vogan†, Molly K. Wagner*, Clifford J. Tabin†, H. Joseph Yost*, Martina Brueckner‡

**Center for Children, Huntsman Cancer Institute and Department of Oncological Sciences, University of Utah, Salt Lake City, Utah 84112-5550, USA*
e-mail: joseph.yost@hci.utah.edu
†Department of Genetics, Harvard Medical School, Boston, Massachusetts 02115, USA
‡Department of Pediatrics and Cardiology, Boyer Center for Molecular Medicine, Yale University School of Medicine, New Haven, Connecticut 06520, USA

1. Capdevila, J. *et al. Cell* **101,** 9–21 (2000).
2. Wright, C. V. E. *Dev. Cell* **1,** 179–186 (2001).
3. Nonaka, S. *et al. Cell* **95,** 829–837 (1998).
4. Okada, Y. *et al. Mol. Cell* **4,** 459–468 (1999).
5. Supp, D. M. *et al. Nature* **389,** 963–966 (1997).
6. Supp, D. M. *et al. Development* **126,** 5495–5504 (1999).
7. Olbrich, H. *et al. Nature Genet.* **30,** 143–144 (2002).
8. Männer, J. *Anat. Embryol.* **203,** 481–490 (2001).
9. Cooper, M. S. & D'Amico, L. A. *Dev. Biol.* **180,** 184–198 (1996).

Supplementary information accompanies this communication on *Nature*'s website.
Competing financial interests: declared none.

Gene expression

RNA interference in adult mice

RNA interference is an evolutionarily conserved surveillance mechanism that responds to double-stranded RNA by sequence-specific silencing of homologous genes. Here we show that transgene expression can be suppressed in adult mice by synthetic small interfering RNAs and by small-hairpin RNAs transcribed *in vivo* from DNA templates. We also show the therapeutic potential of this technique by demonstrating effective targeting of a sequence from hepatitis C virus by RNA interference *in vivo*.

Small interfering RNAs (siRNAs) mimic intermediates in the RNA-interference (RNAi) pathway and can silence genes in somatic cells without activating non-specific suppression by double-stranded RNA-dependent protein kinase[1]. To investigate whether siRNAs also inhibit gene expression *in vivo*, we used a modification of hydrodynamic transfection methods[2–4] to deliver naked siRNAs to the livers of adult mice. Either an siRNA derived from firefly luciferase or an unrelated siRNA was co-injected with a luciferase-expression plasmid (for construct description and sequences, see supplementary information). We monitored luciferase expression in living animals using quantitative whole-body imaging[5] (Fig. 1a, c), and found that it was dependent on reporter-plasmid dose (results not shown).

In each experiment, serum measurements of a co-injected human α-1 antitrypsin (hAAT) plasmid[6] served to normalize transfection efficiency and to monitor non-specific translational inhibition. Average serum concentrations of hAAT after 74 h were similar in all groups.

Our results indicate that there was specific, siRNA-mediated inhibition of luciferase expression in adult mice ($P < 0.0115$) and that unrelated siRNAs had no effect ($P < 0.864$; Fig. 1a, b). In 11 independent experiments, luciferase siRNAs reduced luciferase expression (as judged by emitted light) by an average of 81% (±2.2%). These findings indicate that RNAi can downregulate gene expression in adult mice.

As RNAi degrades respiratory syncitial virus RNAs in culture[7], we investigated whether RNAi could be directed against a human pathogenic RNA expressed in a mouse, namely that of hepatitis C virus (HCV). (Infection by HCV, an RNA virus that infects 1 in 40 people worldwide, is the most common reason for liver transplantation in the United States and Europe.) We fused the NS5B region (non-structural protein 5B, viral-polymerase-encoding region) of this virus with luciferase RNA and monitored RNAi by co-transfection *in vivo*. An

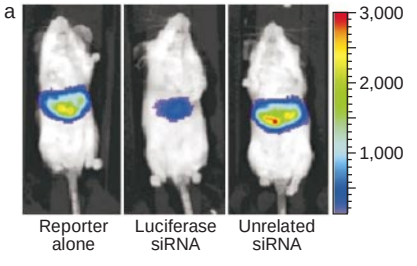

Figure 1 RNA interference in adult mice. **a,** Representative images of light emitted from mice co-transfected with the luciferase plasmid pGL3-control and either no siRNA, luciferase siRNA or unrelated siRNA. A pseudocolour image representing intensity of emitted light (red, most intense; blue, least intense) superimposed on a greyscale reference image (for orientation) shows that RNAi functions in adult mice. Annealed 21-nucleotide siRNAs (40 μg; Dharmacon) were co-injected into the livers of mice with 2 μg pGL3-control DNA (Promega) and 800 units of RNasin (Promega) in 1.8 ml PBS buffer in 5–7 s. After 72 h, mice were anaesthetized and given 3 mg luciferin intraperitoneally 15 min before imaging. **b,** siRNA results (six mice per group) from a representative experiment. Mice receiving luciferase siRNA emitted significantly less light than reporter-alone controls (one-way ANOVA with post hoc Fisher's test). Results for reporter alone and unrelated siRNA were statistically similar. **c,** pShh1-Ff1, but not pShh1-Ff1rev (see text), reduced luciferase expression in mice relative to the reporter-alone control. pShh1-Ff1 or pShh1-rev (10 μg) were co-injected with 2 μg pGL3-control in 1.8 ml PBS buffer. **d,** Average of three independent shRNA experiments ($n = 5$). Average values for the reporter-alone group are designated as 100% in each of the three experiments. Animals were treated according to the US National Institutes of Health's guidelines for animal care and the guidelines of Stanford University.

siRNA targeting the NS5B region reduced luciferase expression from the chimaeric HCV NS5B protein–luciferase fusion by 75% (±6.8%; 6 animals per group). This result suggests that it may be feasible to use RNAi as a therapy against other important human pathogens.

Although our results show that siRNAs are functional in mice, delivery remains a major obstacle. Unlike siRNAs, functional small-hairpin RNAs (shRNAs) can be expressed *in vivo* from DNA templates using RNA polymerase III promoters[8,9]; they are as effective as siRNAs in inducing gene suppression. Expression of a cognate shRNA (pShh1-Ff1; see supplementary information) inhibited luciferase expression by up to 98% (±0.6%), with an average suppression of 92.8% (±3.39%) in three independent experiments (Fig. 1c, d). An empty shRNA-expression vector had no effect (results not shown); reversing the orientation of the shRNA (pShh1-Ff1rev) insert prevents gene silencing because it alters the termination by RNA polymerase III and generates an improperly structured shRNA. These findings indicate that plasmid-encoded shRNAs can induce a potent and specific RNAi response in adult mice.

RNAi may find application in functional genomics or in identifying targets for designer drugs. It is a more promising system than gene-knockout mice because groups of genes can be simultaneously rendered ineffective without the need for time-consuming crosses. Gene therapy currently depends on the ectopic expression of exogenous proteins; however, RNAi may eventually complement this gain-of-function approach by silencing disease-related genes with DNA constructs that direct the expression of shRNAs. Our method of RNAi delivery could also be tailored to take advantage of developing viral and non-viral gene-transfer vectors in a clinical context.

Anton P. McCaffrey*, Leonard Meuse*, Thu-Thao T. Pham*, Douglas S. Conklin†, Gregory J. Hannon†, Mark A. Kay*

**Departments of Pediatrics and Genetics, Stanford University School of Medicine, Stanford, California 94305-5208, USA*
e-mail: markay@stanford.edu
†Cold Spring Harbor Laboratory, 1 Bungtown Road, Cold Spring Harbor, New York 11724, USA

1. Elbashir, S. M. *et al. Nature* **411,** 494–498 (2001).
2. Zhang, G., Budker, V. & Wolff, J. A. *Hum. Gene Therapy* **10,** 1735–1737 (1999).
3. Liu, F., Song, Y. & Liu, D. *Gene Therapy* **6,** 1258–1266 (1999).
4. Chang, J., Sigal, L. J., Lerro, A. & Taylor, J. *J. Virol.* **75,** 3469–3473 (2001).
5. Contag, C. H. *et al. Photochem. Photobiol.* **66,** 523–531 (1997).
6. Yant, S. R. *et al. Nature Genet.* **25,** 35–41 (2000).
7. Bitko, V. & Barik, S. *BMC Microbiol.* **1,** 34 (2001).
8. Paddison, P. J., Caudy, A. A., Bernstein, E., Hannon, G. J. & Conklin, D. S. *Genes Dev.* **16,** 948–958 (2002).
9. Tuschl, T. *Nature Biotechnol.* **20,** 446–448 (2002).

Supplementary information accompanies this communication on *Nature*'s website.

Competing financial interests: declared none.

COMMUNICATIONS ARISING

Orbital physics

Experimental quest for orbital waves

One challenge in condensed-matter physics is the experimental confirmation of a new kind of elementary excitation — orbital waves, or orbitons, which are predicted to exist in an orbitally ordered state. Saitoh *et al.*[1] have observed three peaks at 160, 144 and 126 meV in the Raman scattering of orbitally ordered lanthanum manganate ($LaMnO_3$), and interpret these as evidence of orbitons. However, we find similar peaks in the optical conductivity, $\sigma(\omega)$, of $LaMnO_3$ and point out that the direct observation of orbitons in $\sigma(\omega)$ is prohibited by a selection rule. This suggests that the Raman peaks observed by Saitoh *et al.* arise from multiphonons, and that the existence of orbitons has yet to be experimentally confirmed.

We determined $\sigma(\omega)$ by measuring both the transmittance and reflectance of single crystals, using a sample polished to a thickness of $d \approx 62$ μm for the former. We compared $\sigma(\omega)$ of $LaMnO_3$ with the Raman data of Saitoh *et al.*[1] and found that the peaks in $\sigma(\omega)$ were similar to the Raman features (Fig. 1, top), albeit with slightly different frequencies (160, 146, 130 and 118 meV).

The orbital excitations discussed by Saitoh *et al.* involve transitions between orbital states of the same parity. These transitions do not contribute directly to $\sigma(\omega)$ owing to the parity selection rule; that is, they are not infrared-active. They may become weakly infrared-active in the presence of defects or by the simultaneous excitation of a parity-breaking Mn–O bond-stretching phonon[2]. The latter, phonon-activated mechanism is the more effective way to break the selection rule. Stronger features are therefore expected in $\sigma(\omega)$ at frequencies that — compared to the Raman peaks — are shifted by the respective phonon frequency of about 70 meV. As this is not the case, the peaks in $\sigma(\omega)$ cannot be explained by orbitons, challenging the orbiton interpretation of the Raman data.

We suggest that all peaks should be interpreted as arising from multiphonons. The sharp increase in $\sigma(\omega)$ at low frequen-

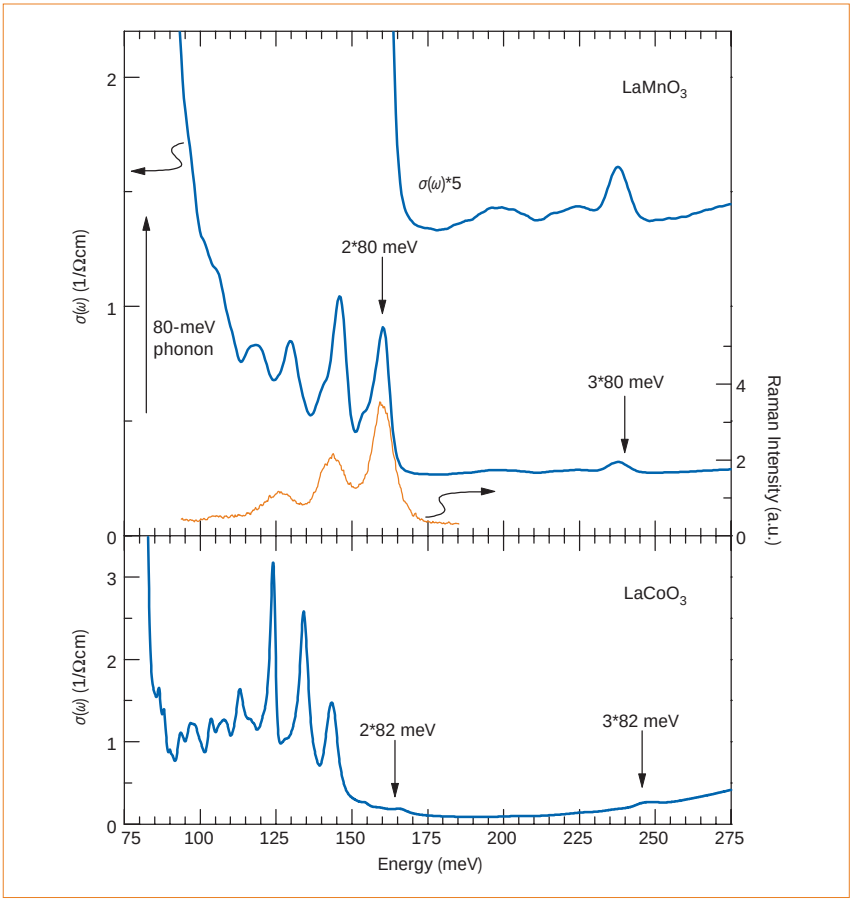

Figure 1 Optical conductivity $\sigma(\omega)$ of $LaMnO_3$ and $LaCoO_3$, and Raman measurements on $LaMnO_3$ at a temperature of 4 K. Top, comparison of $\sigma(\omega)$ (thick blue line) and Raman intensity (from Saitoh *et al.*[1]; thin yellow line) of $LaMnO_3$ reveals a close similarity between the two spectra. In $\sigma(\omega)$ the highest peaks of single-, two- and three-phonon absorption are observed at 80, 160 and 240 meV, respectively. Inset, enlargement of the three-phonon range of $\sigma(\omega)$. Bottom, $\sigma(\omega)$ of $LaCoO_3$, showing multiphonon peaks, for example at 2*82 and 3*82 meV.